Journal Pre-proofs

Extraction of Glabridin from Glycyrrhiza glabra L. root using ethanol modified supercritical CO2: RSM optimization and mathematical modeling

Ali Hedayati , S. M. Ghoreishi

DOI: https://doi.org/ 10.22104/ift.2026.8092.2264

To appear in: Innovative Food Technologies (IFT)

Received Date: 29 December 2025
Revised Date: 1 February 2026
Accepted Date: 7 February 2026

Please cite this article as: Ali Hedayati , S. M. Ghoreishi, Extraction of Glabridin from Glycyrrhiza glabra L. root using ethanol modified supercritical CO2: RSM optimization and mathematical modeling, *Innovative Food Technologies (2026)*, doi: https://doi.org/ 10.22104/ift.2026.8092.2264

Extraction of Glabridin from *Glycyrrhiza glabra* L. root using ethanol modified supercritical CO_2: RSM optimization and mathematical modeling

Ali Hedayati [a,*], S. M. Ghoreishi [b]

[a] *Department of Chemical Technologies, Iranian Research Organization for Science and Technology (IROST), Tehran, Iran*

[b] *Department of Chemical Engineering, Isfahan University of Technology, Isfahan, Iran*

**Corresponding Author Email: a.hedayati@irost.ir*

Abstract

In this study, supercritical fluid extraction (SFE) of glabridin (GB) from licorice (*Glycyrrhiza glabra* L.) roots was carried out using CO_2 as the solvent and ethanol as a co-solvent. Response surface methodology (RSM) was employed for the design of experiments (DOEs), modeling and optimization of GB extraction recovery. Temperature (40-80 °C), pressure (8-24 MPa), CO_2 flow rate (0.5-2.5 ml/min) and dynamic extraction time (20-100 min) were considered as independent operating variables. At all experiments the static extraction time and co-solvent flow rate were kept constant at 30 min and 5 vol. % of the CO_2 flow rate, respectively. The GB content in the extracted samples was quantified using high-performance liquid chromatography (HPLC). The maximum extraction recovery of 60±2% was obtained at the optimal conditions of 40 °C, 24 MPa, 1.8 ml CO_2/min and 76 min. The isotherms of GB recovery were also obtained as a function of time at 24 MPa and a CO_2 flow rate of 1.8 mL min^{-1}. Moreover, a mechanistic mass-transfer model incorporating solid-fluid equilibrium, interphase mass transfer, axial dispersion and intraparticle diffusion was developed to describe the extraction kinetics. The developed model successfully predicted the experimental data with an overall average absolute relative deviation (AARD) of approximately 4.2%.

Keywords: Supercritical CO_2; Extraction; Glabridin; Response surface methodology (RSM); *Glycyrrhiza glabra* (licorice); Co-solvent (modifier); Mathematical Modeling.

1- Introduction

Glycyrrhiza glabra, commonly known as licorice, is a perennial herb from the Fabaceae family [1], cultivated worldwide for its roots and rhizomes rich in bioactive compounds such as triterpenoid saponins and phenolics [2]. Licorice exhibits diverse medicinal properties, including antitumor [3], antioxidant [4], antimicrobial [5], anti-inflammatory [6], anti-diabetic [7] and hepatoprotective effects [8] and its extracts are widely used as natural sweeteners and flavoring agents in food and pharmaceutical industries [9]. Glabridin (GB, Fig. 1) is a hydrophobic isoflavane and is used in cosmetics, food, and traditional medicine [10], showing multiple pharmacological activities such as anti-oxidative [11], anti-tumorigenic [12], anti-inflammatory [13], antimicrobial [14], neuroprotective [15], skin-whitening [16], and estrogenic effects [17].

The pharmacological significance of GB has led to extensive studies on its extraction from licorice using various solvents (methanol, ethanol, water, ethyl acetate), procedures (dipping, Soxhlet, ultrasonic-assisted, enzymatic), and conditions, yielding 0.03–0.92 mg/g depending on method and source [18, 19]. Solid-phase extraction [20], molecularly imprinted polymers [21] and ionic liquids [22] have also been applied for purification. Recent green approaches such as ultrasound-assisted deep eutectic solvent extraction (DES-UAE) [23] and ultrasound-assisted aqueous two-phase extraction (UA-ATPE) [24] improved GB recovery, selectivity and reduced extraction time and solvent toxicity. However, SC-CO_2 offers an eco-friendly alternative with tunable selectivity, high solvation power and low toxicity, though co-solvents are often required to extract polar compounds effectively [25, 26].

SFE has been used in a number of studies for the GB extraction from licorice root. SFE of GB from *G. glabra* was carried out by Ahn et al. [27] at the extraction pressure of 30 MPa, the temperature of 40 °C, extraction time of 1 h and CO_2 flow rate of 150 g/min. The amount of extracted GB was determined to be 1.61 mg/g licorice. Sohail et al. [28] extracted GB from licorice according to the procedure of Ahn et al. [27] at 40 °C, 3h and three different pressures of 24.1, 31.0 and 37.9 MPa such that the maximum extraction was obtained to be 2.97 mg/g licorice at the maximum pressure. Hong et al. [29] employed ethanol-modified SC-CO_2 extraction to obtain GB-enriched licorice extracts and by combining SFE with sequential alcohol precipitation and adsorption chromatography, increased GB purity from 6.2% to about 37%.

Introducing an efficient method in terms of GB selectivity is very important to reduce the subsequent efforts for its isolation from other components of the natural source. So far, there is no published study reporting a comprehensive investigation and optimization of supercritical extraction of GB from *Glycyrrhiza glabra* L. root. Hence, implementation of modified SC-CO_2 for GB extraction and optimization of operating variables including pressure, temperature, dynamic extraction time and CO_2 flow rate is the main objective of this study. Ethanol generally recognized as safe (GRAS) and an environmental benign solvent selected as co-solvent to increase the solvation power by improving the fluid affinity toward polar compounds. RSM was used for the DOEs, modeling and optimization of operating conditions, while GB extraction recovery was chosen as the independent variable.

Direct measurement of solute concentration profiles during SFE is difficult under high-pressure conditions. Therefore, validated mathematical models are commonly used to predict extraction behavior [30]. The optimization of operating conditions requires accurate modeling of phase behavior, mass transfer, and equilibrium phenomena [31]. In this work, a differential mass balance model [32] was implemented for GB extraction from licorice using modified SC-CO_2 and the effects of temperature, pressure, flow rate and extraction time were systematically analyzed.

2- Experimental

2-1- Materials

Glycyrrhiza glabra L. (licorice) roots were obtained from the Iranian Research Institute of Plant Protection (IRIPP). The plants were harvested at full maturity (approximately 3-4 years old) and only the main roots were used in this study, while fine lateral roots were removed to ensure sample homogeneity. The licorice material was obtained from a single batch to minimize biological variability. The roots were air-dried, crushed, and sieved to a particle size range of 20-35 mesh (0.841-0.507 mm) prior to extraction. Carbon dioxide (purity >99.5%, Ardestan) and ethanol (purity ≥99.9%, Merck) were used in the SFE process. Methanol (purity ≥99.9%, Merck), acetic acid (purity ≥99.8%, Merck), deionized water, and glabridin (GB, purity ≥98%, Sigma-Aldrich) were used for HPLC analysis.

2-2- Supercritical fluid extraction apparatus

Fig. 2 shows the experimental set-up for the SFE process in this study. Combined static and dynamic extraction method was performed similar to our previous publications [33, 34]. Briefly, the equipment comprised of: (1) CO_2 cylinder, (2) molecular sieve column to attain maximum CO_2 purity, (3) co-solvent (ethanol) container, (4) HPLC pump (Dionex GS50 Gradient Pump) for co-solvent which adjusted to work at a flow rate equal to 5 vol. % of CO_2 flow rate in every designed experiment, (5) HPLC pump (Jasco, PU-1580) for CO_2, (6) circulating water bath, (7) high pressure needle valves, (8) coil preheater, (9) extraction vessel (volume= 8 cm^3) filled with

2 g of licorice root, (10) oven, (11) back pressure regulator (TESCOM, 26-1762-24) and (12) sample collector. The static extraction time was kept constant at 30 min in all experiments.

Fig. 2: Schematic of experimental set-up for SFE; (1) CO_2 cylinder, (2) molecular sieve column, (3) co-solvent container, (4) co-solvent pump, (5) CO_2 pump, (6) chiller, (7) high pressure needle valves, (8) spring coil preheater, (9) extraction vessel, (10) oven, (11) back pressure regulator, (12) extract collector.

2-3- Glabridin quantification

The concentration of GB in the extracted samples was obtained by HPLC. GB was analyzed by Venusil MP C18 column (length =300 mm, internal diameter=3.9 mm and stationary phase thickness=10 µm) with a mobile phase of methanol/water (3 vol. % acetic acid) with a volume ratio of 41/59 (v/v). Mobile phase flow rate, temperature, injection volume and detector were chosen to be 1 ml/min, ambient temperature, 20 µL and UV detector (wavelength= 48 nm), respectively. Linear regression of peak area versus concentration of standard aqueous GB solutions was used to determine the calibration curve ($y = 85.788x - 2820.3$, $R^2=0.997$). Fig. 3 illustrates the chromatogram of an extracted sample by SFE.

Fig. 3: chromatogram of an extracted sample by SFE (inset of figure shows the chromatogram of standard GB).

2-4- Design of experiments

The conventional procedure for the optimization of operating conditions is one factor at a time (OFAT) method. In this method, the effect of one parameter on an independent variable is evaluated while other variables have been kept constant. The main disadvantages of OFAT method are: ignoring the interaction effects among operating variables and necessity for the higher number of experiments which is costly and time-consuming [35].

Above mentioned drawbacks led to the implementation of RSM [36] as a statistical tool for the DOEs, modeling, optimization and investigation of the effect of operating conditions on the GB extraction recovery.

Central composite rotatable design (CCRD) with four independent variables including pressure (8-24 MPa), temperature (40-80 °C), CO_2 flow rate (0.5-2.5 ml/min) and dynamic extraction time (20-100 min) at five levels (Table 1) was applied in RSM using GB extraction recovery as response (independent) variable. Static extraction time was kept constant at 30 min based on the preliminary results for all designed experiments. Also, the co-solvent (ethanol) flow rate was adjusted to be equal to 5 vol. % of the CO_2 flow rate to assure single phase extraction in each experiment.

Experimental replication was incorporated through repeated center points in the design, which were used to estimate the pure experimental error and assess model adequacy. The optimum extraction condition predicted by the RSM model was validated by performing three independent extractions and the reported result represents the mean ± standard deviation.

Table 1: Independent variables in RSM based on coded and uncoded levels.

Table 2 shows 30 designed experiments (full factorial) using Minitab software as a tool for RSM implementation where the points type are as follows: 16 cube points, 4 center points in cube, 8 axial points and 2 center points in axial.

Table 2: RSM designed experiments for GB extraction from licorice plant root and observed experimental and modeling results.

3- Mathematical modeling

The supercritical extraction process was modeled as a packed bed of licorice root with ethanol-modified SC-CO_2 as the mobile phase, consisting of static and dynamic stages. The extraction behavior was controlled by solid-fluid equilibrium, interphase mass transfer and axial dispersion. The solute release was assumed to proceed via irreversible desorption and intraparticle diffusion and was described by coupled mass balance equations.

The model assumed constant temperature and pressure, invariant fluid properties, single-component solute behavior, spherical and uniformly sized particles, uniform initial solute distribution, constant superficial velocity, and local linear equilibrium between the solid phase and pore fluid. Axial dispersion was considered significant, whereas radial dispersion and radial concentration gradients were neglected due to the small column diameter.

Under these assumptions, the dimensionless mass balance for the mobile phase is given by:

$$\frac{\partial y}{\partial \theta} = \frac{1}{Pe_b}\frac{\partial^2 y}{\partial \zeta^2} - \frac{\partial y}{\partial \zeta} + 6\frac{1-\varepsilon}{\varepsilon}\frac{L}{R_p}\frac{Bi}{Pe_p}(x_{\rho=1} - y) \qquad (1)$$

with the initial and boundary conditions:

$$y(\theta = 0) = 0 \qquad (1a)$$

$$y - \frac{1}{Pe_b}\frac{\partial y}{\partial \zeta} = 0(\zeta = 0) \qquad (1b)$$

$$\frac{\partial y}{\partial \zeta} = 0(\zeta = 1) \qquad (1c)$$

Solute transport within the solid particles was modeled as diffusion in spherical coordinates:

$$\varepsilon_p\frac{\partial x}{\partial \theta} + (1-\varepsilon_p)b\frac{\partial x_s}{\partial \theta} = \frac{2}{Pe_p}\frac{L}{R_p}\frac{1}{\rho^2}\frac{\partial}{\partial \rho}(\rho^2\frac{\partial x}{\partial \rho}) \qquad (2)$$

where $b = C_{s,0}/C_{p,0}$. Assuming a linear equilibrium relationship:

$$x_s = \frac{K_d}{b}x \qquad (3)$$

Eq. (2) reduces to:

$$\frac{\partial x}{\partial \theta} = \frac{\alpha}{\rho^2}\frac{\partial}{\partial \rho}(\rho^2\frac{\partial x}{\partial \rho}) \qquad (4)$$

with $\alpha = \frac{2}{Pe_p}\frac{L}{R_p}\frac{1}{\beta}$ and $\beta = \varepsilon_p + (1-\varepsilon_p)K_d$.

The overall extraction recovery was obtained from a mass balance over the extractor:

$$\frac{dF}{d\theta} = \frac{\varepsilon}{\varepsilon_p + (1-\varepsilon_p)K_d + (1-\varepsilon)}\, y\,|_{\zeta=1} \qquad (5)$$

with the initial condition $F(0) = 0$.

The dimensionless equations (Eqs. (2), (5) and (6)) were solved numerically using an explicit finite difference method. The extractor length and particle radius were discretized into *M* axial and *N* radial nodes, respectively.

Discretization of the mobile-phase mass balance equation (Eq. (2)) yields:

$$\frac{y_{i,n+1} - y_{i,n}}{\Delta\theta} = (\frac{1}{2\Delta\zeta} + \frac{1}{Pe_b\Delta\zeta^2})y_{i-1,n} - (\frac{2}{Pe_b\Delta\zeta^2} + \frac{6LBi}{R_pPe_p}\frac{1-\varepsilon}{\varepsilon})y_{i,n} + (-\frac{1}{2\Delta\zeta} + \frac{1}{Pe_b\Delta\zeta^2})y_{i+1,n} + \frac{6LBi}{R_pPe_p}\frac{1-\varepsilon}{\varepsilon}x_{N,i,n} \qquad (6)$$

with the initial and boundary conditions:

$$y_{i,0} = 0 \qquad (6a)$$

$$y_{0,n} = \frac{4y_{1,n} - y_{2,n}}{3 + 2Pe_b\Delta\zeta} \qquad (6b)$$

$$y_{M,n} = \frac{4}{3}y_{M-1,n} - \frac{1}{3}y_{M-2,n} \qquad (6c)$$

The intraparticle diffusion equation (Eq. (4)) was discretized in spherical coordinates as:

$$\frac{x_{j,i,n+1} - x_{j,i,n}}{\Delta\theta} = \frac{\alpha}{\Delta\rho^2}[(1 - \frac{1}{j})x_{j-1,i,n} - 2x_{j,i,n} + (1 + \frac{1}{j})x_{j+1,i,n}] \qquad (7)$$

with the following conditions:

$$x_{j,i,0} = 1 \qquad (7a)$$

$$x_{0,i,n} = \frac{4}{3}x_{1,i,n} - \frac{1}{3}x_{2,i,n} \qquad (7b)$$

$$x_{N,i,n} = \frac{4x_{N-1,i,n} - x_{N-2,i,n} + 2Bi\,\Delta\rho\, y_{i,n}}{3 + 2Bi\,\Delta\rho} \qquad (7c)$$

The extraction recovery equation (Eq. (5)) was discretized using a forward difference scheme:

$$\frac{F_{n+1} - F_n}{\Delta\theta} = \frac{\varepsilon}{\varepsilon_p + (1 - \varepsilon_p)K_d + (1 - \varepsilon)}\, y_{M,n} \qquad (8)$$

with the initial condition:

$$F_0 = 0 \qquad (8a)$$

The resulting coupled equations were solved to concentration profiles in both phases and the overall extraction recovery.

Model parameters include the thermophysical properties of the mixture (density and viscosity), molecular diffusivity, axial dispersion coefficient, external mass transfer coefficient and the solid-fluid equilibrium constant. The density of the CO_2-water mixture was calculated as [37]:

$$\rho_m = \frac{M_1y_1 + M_2y_2}{v_m} \qquad (9)$$

where $M_i$and $y_i$are the molecular weight and mole fraction of CO_2 and ethanol. The molar volume was obtained from $v_m = ZRT/P$, where the compressibility factor Z was calculated using the Peng-Robinson equation of state with van der Waals mixing rules [38].

The viscosity of the dense gas mixture was estimated using the Chung method [39]. The mixture diffusion coefficient was calculated as [57]:

$$D_m = (D_1D_2)^{0.5} \qquad (10)$$

where the solute diffusivity in SC-CO_2 was estimated using the He-Yu correlation [40].

The axial dispersion coefficient was evaluated as:

$$D_{ax} = \frac{ud_p}{Pe_c} \qquad (11)$$

where the Peclet number was obtained from the Ghoreishi-Akgerman correlation [41]:

$$\frac{1}{Pe_c} = \frac{0.3}{Re\,Sc} + \frac{0.5}{1 + 3.8/(Re\,Sc)} \qquad (12)$$

with $Re = 2\varepsilon R_p\rho_m u/\eta_m$and $Sc = \eta_m/(\rho_m D_m)$.

The external mass transfer coefficient was calculated as:

$$k_f = \frac{ShD_{\text{eff}}}{2R_p} \qquad (13)$$

where the Sherwood number was obtained from [42]:

$$Sh = 0.38Re^{0.83}Sc^{0.33} \qquad (14)$$

The effective intraparticle diffusivity was estimated using the Wakao correlation [43]:

$$D_{\text{eff}} = \varepsilon_p^2 D_m \qquad (15)$$

The solid-fluid distribution coefficient was defined as [44]:

$$K_d = \frac{(W_{GB}/W_s)}{(W_{GB}/V_m)}\,\rho_s \qquad (16)$$

where the solute concentration in the mobile phase was calculated as:

$$\frac{W_{GB}}{V_m} = \frac{M_k y_k}{v_m} = S \qquad (17)$$

The bed length, bed diameter, particle diameter, bed porosity and particle porosity were 0.125 m, 0.009 m, 0.000674 m, 0.45, and 0.12, respectively. Particle-related parameters were obtained experimentally.

The recovery data from the designed experiments by RSM and the obtained isotherms for recovery at the optimum pressure and flow rate versus extraction time were used for the regression of GB solubility in SC-CO_2 (S) (Eq. (18)), GB critical properties (Tc, Pc, ω) and binary interaction parameters ($l_{ethanol\text{-}GB}$, $l_{CO2\text{-}GB}$).

$$S = a + b\,T + cP + dT^2 + eP^2 + fT.P \qquad (18)$$

The adjustable parameters for each were regressed by simultaneous fitting the recovery using the following objective function (OF):

$$AAD\% = \frac{1}{NP}\sum_{i=1}^{NP}\left|\frac{R_{exp,i} - R_{model,i}}{R_{exp,i}}\right| \times 100 \qquad (19)$$

4- Results and Discussion

The GB extraction recoveries in Table 2 were calculated according to Eq. (1):

$$R_{GB} = \frac{Y_{GB}^{SFE}}{Y_{GB}^{Sox}} \times 100 \qquad (20)$$

Where R_{GB}, Y_{GB}^{SFE} and Y_{GB}^{Sox} are GB extraction recovery, GB extraction yield in SFE process (mg GB/gr licorice) and GB extraction yield in Soxhlet extraction (mg GB/gr licorice), respectively. It was considered that the total extractable GB can be achieved by Soxhlet using ethanol/water (70:30, v/v) as solvent for 16 h. The GB extraction yield was determined via triplicate experiments to be 1.8±0.2 mg GB/gr dried licorice root.

4-1- RSM model for GB extraction recovery

The coefficients of Eq. (21) as a model for GB extraction recovery were calculated based on the responses in Table 2.

$$y = a_0 + \sum_{i=1}^{k} a_i x_i + \sum_{i=1}^{k} a_{ii} x_i^2 + \sum_{i}\sum_{j} a_{ij} x_i x_j + \varepsilon \qquad (21)$$

Where the number of operating variables, constant of second-order polynomial equation, residual associated with the experiments, coefficients of linear, quadratic and interaction terms were identified by k, ε, a_0, a_i, a_{ii} and a_{ij}, respectively. Independent coded variables (x_i) are defined by the following equation:

$$x_i = \frac{z_i - z_{i.CP}}{\Delta\theta} \qquad (22)$$

Where x_i, z_i, $z_{i.CP}$ and $\Delta\theta$ are the value of coded variable, the value of uncoded variable, the value of uncoded variable at center point and step change in the x_i.

The regression coefficients of the 2nd order polynomial model (Eq. (21)) were provided in Table 3. Analysis of variance (ANOVA) was also carried out as a method for model validation (Table 3).

Table 3: Regression coefficients and ANOVA of the second-order polynomial model for GB extraction recovery.

The importance of each term in the proposed model was determined by statistical p-value. The terms of model with $p<0.001$, $0.001\leq p<0.05$ and $p\geq 0.05$ were regarded as the highly significant, significant and insignificant, respectively. Accordingly, both linear and quadratic terms of pressure (P and P^2) and time (t and t^2) were highly significant ($p<0.001$), while the linear and quadratic terms of CO_2 flow rate (Q and Q^2) were insignificant ($p\geq 0.05$). Moreover, the linear and quadratic terms of temperature (T and T^2) were significant (p-value=0.006) and insignificant (p-value=0.527), respectively. All interaction terms except the interaction terms of $T\times P$ (p-value=0.014) and $P\times t$ (p-value=0.018) were insignificant in the second-order model. Fig. 4 shows the Pareto chart of the standardized effects that can be used to determine the relative effect of model terms on the response variable. Among all model terms, the linear term of pressure had the most important effect on the GB extraction recovery.

Fig. 4: Pareto chart of standardized effects in RSM model for GB extraction recovery.

The regression equation for GB extraction recovery in coded units was determined as follows:

$$R_{GB}^{model} = 23.8 + 1.642T + 10.058P + 1.008Q + 2.725t - 0.304T^2 + 2.533P^2 - 0.617Q^2 - 1.967t^2 - 1.750TP + 0.175TQ - 0.100Tt + 0.137PQ + 1.662Pt - 0.163Qt \quad (23)$$

The calculated standard deviation, coefficient of determination (R^2) (Fig. 5), adjusted coefficient of determination (Adj. R^2) and predicted coefficient of determination (Pred. R^2) were 2.45, 97.49%, 94.57% and 80.40%, respectively which shows the model adequacy.

Fig. 5: Experimental vs RSM predicted GB extraction recovery.

In the following sections, contour and surface plots of process variables are used to evaluate the effects of each term on the response variable (GB extraction recovery).

4-2- Effect of operating conditions on GB extraction recovery

4-2-1- Effect of temperature

Figs. 6-8 illustrate the three-dimensional response surface and contour plots according to Eq. (23) to investigate the effect of temperature versus pressure, CO_2 flow rate and dynamic extraction time on the GB extraction recovery. The surface plots were sketched by assigning z-axis to the GB extraction recovery, while x and y coordinates were used for the two independent variables and the other two independent variables were fixed (Table 1).

As is evidenced in Fig. 6, temperature has counter effects on the GB solubility in SC-CO_2. Increasing temperature reduces the solvation power of SC-CO_2 by decreasing the density of solvent. Simultaneously, the vapor pressure of solute (GB) has a direct relation with temperature. Therefore, a higher temperature leads to the enhanced GB solubility and extraction recovery.

Fig. 6: (a) surface and (b) contour plots for the effect of temperature and pressure on the GB extraction recovery at constant dynamic extraction time and CO_2 flow rate of 60 min and 1.5 ml/min, respectively.

The effect of enhanced vapor pressure is more pronounced than the effect of reduced density below the crossover pressure (the pressure of isotherms intersection). However, beyond the crossover pressure of about 20 MPa (code=1), the influence of decreased density is more important than the effect of higher volatility which results in the decrease of GB extraction recovery by increasing the temperature. However, Figs. 7 and 8 were plotted at zero level of pressure (P=16 MPa), such that the retrograde solubility does not exist. As presented in Table 3, temperature has a significant positive linear effect (effect= 3.27) and an insignificant negative quadratic effect (effect=0.64) on the GB recovery that lowers the rate of raise in recovery at higher temperature levels.

Fig. 7: (a) surface and (b) contour plots for the effect of temperature and CO_2 flow rate on the GB extraction recovery at constant dynamic extraction time and pressure of 60 min and 16 MPa, respectively.

Fig. 8: (a) surface and (b) contour plots for the effect of temperature and dynamic extraction time on the GB extraction recovery at constant CO_2 flow rate and pressure of 1.5 ml/min and 16 MPa, respectively.

4-2-2- Effect of pressure

Figs. 6, 9 and 10 show the interaction effects of pressure versus temperature, CO_2 flow rate and dynamic extraction time, respectively while other variables were kept constant at zero levels. Generally, pressure has dual counter effects on solute extraction recovery in SFE. On one hand, increasing pressure leads to the higher CO_2 density and solvation power. On the other hand, higher SC-CO_2 density, reduces the solvent diffusivity and mass transfer coefficient, therefore, decreasing the solubility and causes lower extraction recovery.

In this study, pressure has highly significant linear (effect= 20.08) and quadratic (effect=5.40) positive effects on the GB extraction recovery (Table 3). Therefore, the positive effect of increased density prevails the negative effect of decreased mass transfer with the addition of pressure in the operating range of this research.

As depicted in Fig. 10, increasing pressure from 8 MPa (code=-2) to 24 MPa (code=2) at constant condition of 60 °C, 60 min and 1.5 ml/min (all in zero levels) leads to the considerable enhancement in GB extraction recovery from 13.8% to 54.0%.

Similar trends for the effect of pressure were also observed by Soheil et al. [43], such that increasing pressure from 24.1 to 37.9 MPa, led to the higher GB extraction from 1.64 to 2.97 mg/gr licorice, albeit, the operating pressures were higher than this study.

Fig. 9: (a) surface and (b) contour plots for the effect of pressure and CO_2 flow rate on the GB extraction recovery at constant temperature and dynamic extraction time of 60 °C and 60 min, respectively.

Fig. 10: (a) surface and (b) contour plots for the effect of pressure and dynamic extraction time on the GB extraction recovery at constant temperature and CO_2 flow rate of 60 °C and 1.5 ml/min, respectively.

4-2-3- Effect of CO_2 flow rate

CO_2 flow rate has two opposite effects on the GB extraction recovery. As depicted in Fig. 11, increasing the CO_2 flow rate from 0.5 ml/min (code=-2) to 1.91 ml/min (code=0.83) while other variables were kept constant at 16 MPa, 60 min and 60 °C, increases the GB extraction recovery from 19.3% to 24.2% which is due to the reduced film thickness and mass transfer resistance

around the solid particles of licorice root in the SFE process. Moreover, additional increase in CO_2 flow rate from 1.91 ml/min to 2.5 ml/min (code=2) has a contradictory effect on extraction recovery such that the recovery decreases from 24.2% to 23.4%. Also, Table 3 shows that flow rate has an insignificant positive linear effect (effect=2.01) and an insignificant negative quadratic effect (effect=1.31) on the GB recovery. The negative effect of flow rate at higher levels is because of the reduced residence time of solvent in the extraction vessel that overcomes the positive effect of decreased mass transfer resistance. Furthermore, the effect of CO_2 flow rate versus temperature (fixed dynamic extraction time and pressure at zero levels) and pressure (fixed dynamic extraction time and temperature at zero levels) has been shown in Figs. 7 and 9, respectively. The dual counter effects of flow rate can also be seen in these figures.

Fig. 11: (a) surface and (b) contour plots for the effect of dynamic extraction time and CO_2 flow rate on the GB extraction recovery at constant temperature and pressure of 60 °C and 16 MPa, respectively.

4-2-4- Effect of dynamic extraction time

Dynamic extraction time has a highly significant positive linear effect (effect=5.44) on the GB extraction recovery. Passing fresh SC-CO_2 through the plant matrix at the beginning of process results in the extraction of easily accessible solutes that enhances the extraction recovery. Increasing the dynamic extraction time from 20 min (code=-2) to 67 min (code=0.71) leads to the higher extraction recovery from 10.5% to 24.6% while other variables were at the zero levels (code=0).

At higher levels of extraction time, the rate of extraction is mostly controlled by diffusion rather than convection which leads to the lower GB extraction. This negative effect can also be observed by the highly important quadratic negative effect (effect=4.19) of dynamic extraction time in Table 3. Finally, the optimum extraction time was chosen where there was no sensible change in GB extraction recovery (i.e. 67 min in Fig. 11). It should be noted that the decreased recovery after the optimum extraction time in RSM model (Figs. 8, 10 and 11) is due to the fitting of a quadratic equation to the experimental data.

The interaction plots (Fig. 12) and ANOVA (Table 3) represented that among all interaction terms, only the interaction terms of $P \times T$ (effect=2.85) and $P \times t$ (effect=2.71) had significant effects on the recovery.

Fig. 12: interaction plots of different independent variables.

4-3- Determination of optimum operation conditions

The proposed model (Eq. (23)) for GB extraction recovery was used to determine the optimum extraction condition. Accordingly, the maximum recovery of 61.7% was achieved at the temperature of 40 °C, the pressure of 24 MPa, the CO_2 flow rate of 1.8 ml/min and the dynamic extraction time of 76 min. The optimal point was validated by triplicate experiments which resulted in the GB extraction recovery of 60±2%.

The maximum GB recovery offers valuable insights when compared to prior investigations. Our results align with the general trends observed in the literature, though variations in operating ranges highlight distinct extraction behaviors. In our study, pressure exhibited a dominant positive effect on recovery, with the optimum identified at the upper limit of the design space (24 MPa). This trend is consistent with findings by Sohail et al. [28], who investigated GB extraction at pressures ranging from 3,500 psi (~24 MPa) to 5,500 psi (~38 MPa). They reported that GB yield increased from 1.64 mg/g at 24 MPa to 2.97 mg/g at 38 MPa. While our design space

identified an optimum at 24 MPa, the work by Sohail et al. [28] suggests that extending the pressure range could further enhance yield by maximizing the density and solvation power of the supercritical fluid. Mechanistically, the positive linear and quadratic effects of pressure observed in our model confirm that within this range, the increase in SC-CO_2 density dominates over the decrease in diffusivity, thereby enhancing the solubility of the polar solute.

The recovery achieved in this work (60%) must be contextualized against studies utilizing higher modifier concentrations. Hong et al. [29] reported significantly higher glabridin recoveries (>90%) and extraction rates but utilized a substantially higher ethanol co-solvent concentration of 25% (v/v) compared to the 5% (v/v) used in this study. While higher co-solvent fractions enhance the polarity of the fluid and local interaction with the solute, they may compromise the selectivity of the process and move away from the principles of green chemistry by increasing solvent consumption.

Hong et al. [29] demonstrated that increasing co-solvent concentration from 10% to 25% sharply increased the extraction rate in the initial phases. Our lower recovery can thus be attributed to the limitation of using only 5% ethanol; however, this results in a process with reduced organic solvent requirements.

The trends observed for temperature and flow rate in this study can be explained by competing mechanistic phenomena:

- Temperature: The counter-effect of temperature observed (where higher temperatures can increase vapor pressure but decrease solvent density) is a known phenomenon in SFE. As noted in comparative literature, the crossover pressure determines which factor dominates. In our optimal region, the density effect remains critical for maintaining solvation power.
- Flow Rate: The dual effect of flow rate where recovery increases up to 1.8 mL/min and then decreases, reflects the balance between mass transfer and residence time. Initially, higher flow reduces external mass transfer resistance (film thickness); however, excessive flow rates reduce the residence time of the solvent in the bed, preventing the establishment of equilibrium, a phenomenon also suggested by the plateauing extraction rates in dynamic systems.

Finally, while conventional solvent extraction (CSE) can yield high total mass, SFE offers superior selectivity. Hong et al. [29] noted that SFE achieved a glabridin purity of 6.2%, which was approximately 24 times higher than that obtained via liquid-solid extraction (LSE). Similarly, Ahn et al. [27] confirmed that SFE provides a clean, non-toxic extract with high specific bioactivity, effectively inhibiting adipogenesis markers. Therefore, the 60% recovery obtained in this study represents a high-quality, glabridin-enriched fraction suitable for applications where solvent residue and purity are critical concerns.

4-4- Model validation

The isotherms of GB recovery as a function of time at 24 MPa and a CO_2 flow rate of 1.8 mL min^{-1} and the data in Table 2 were used to regress the model parameters and to evaluate the validity of the developed model (Fig. 13). The overall average absolute relative deviation (AARD) between the experimental data and model predictions was approximately 4.2%, indicating excellent agreement and confirming the robustness of the proposed model over the investigated temperature and time ranges. The regressed critical properties of GB were obtained as $T_c = 1211$ K, $P_c = 2.89$ MPa, and $\omega = 0.92$. The binary interaction parameters involving GB were regressed as $k_{\text{ethanol–GB}} = -0.05$ and $k_{\text{CO}_2\text{–GB}} = 0.15$. For the CO_2-ethanol pair, the binary

interaction parameter in the Peng-Robinson equation of state with the van der Waals quadratic mixing rule has been reported by Mehl et al. [61] as $k_{CO_2-ethanol} \approx 0.084$ near 318 K. The parameters of Eq. (18) used to correlate GB solubility in ethanol-modified SC-CO_2 were determined as $a = 21.46$, $b = -0.746$, $c = 4.142$, $d = -5.63$, and $e = -2.506$.

Fig. 13: Effect of temperature on GB extraction recovery: comparison between experimental data and model predictions.

5- Conclusions

Ethanol modified SC-CO_2 and Soxhlet were implemented for the extraction of GB from licorice plant root. Licorice extract is a complex mixture of various compounds. In order to reduce the time and cost for GB isolation from licorice extract, the operating conditions of SFE process were optimized using RSM. The independent variables were chosen to be temperature, pressure, CO_2 flow rate and dynamic extraction time. GB extraction recovery was selected as the response variable in the DOEs. Analysis of RSM showed that linear terms of pressure and time, as well as the quadratic term of pressure, had a highly significant effect in the proposed model for GB extraction recovery. R^2 and Adj. R^2 of model was determined to be 97.49%, 94.57%, respectively which is an indication of model adequacy. Moreover, the linear term of temperature and interaction terms of $P \times T$ and $P \times t$ were significant. The maximum extraction recovery of 60±2% was obtained at 40 °C, 24 MPa, and 1.8 ml CO_2/min for 76 min. Therefore, modified SC-CO_2 can be used as a green, non-destructive, selective and fast technique for the extraction of GB from licorice plant root.

Beyond RSM optimization, a mechanistic mathematical model was developed to describe the extraction kinetics by incorporating solid-fluid equilibrium, external mass transfer, axial dispersion and intraparticle diffusion phenomena. Thermodynamic properties of the ethanol-modified supercritical phase were evaluated using the Peng-Robinson equation of state and key model parameters including GB solubility, pseudo-critical properties and binary interaction parameters were regressed using experimental recovery-time isotherms. The developed model demonstrated excellent predictive performance, with an overall average absolute relative deviation (AARD) of approximately 4.2% between experimental data and model predictions over a wide range of temperatures and extraction times.

Acknowledgments

The financial support provided by Isfahan University of Technology (IUT) and Iranian Research Organization for Science and Technology (IROST) is gratefully acknowledged.

Nomenclature and units

Bi	Biot number, $(k_f R_p)/D_{eff}$
D_{ax} (m^2/s)	axial dispersion coefficient
D_{eff} (m^2/s)	effective molecular diffusivity of mixture
K_d	solute equilibrium constant between solid and fluid phase in pores
k_f (m/s)	mass transfer coefficient
L (m)	extractor length
Pe_b	Peclet number for the bed, $(Lu)/D_{ax}$
Pe_p	Peclet number for the particle, $(ud_p)/D_{eff}$
Pec	Peclet number, dimensionless, (ud_p/D_{ax})
Re	Reynolds number, $(2R_p u \rho_f \varepsilon)/\mu_f$

R_p(m)	particle radius
Sc	Schmidt number, $\mu_f/\rho_m D_m$
Sh	Sherwood number, $(2R_p k_f)/D_{eff}$
x_s	dimensionless solid phase concentration, C_s/C_{s_0} where C_s is GA concentration in the licorice root
x	dimensionless SCF concentration in the licorice root pore ,C_p/C_{p_0} where C_p is GA concentration in the pore of licorice root
y	dimensionless SCF concentration, C_b/C_{b_0} where C_b is GA concentration in the mobile phase
Z (m)	axial distance
A_0	Constant
A_i	Coefficient of linear parameters
A_{ii}	Coefficient of quadratic parameters
A_{ij}	Coefficient of interaction parameters
k	Number of variables
P(MPa)	extraction pressure
Q(ml/min)	CO_2 flow rate
R (%)	Recovery
t(min)	Dynamic extraction time
T(°C)	Extraction temperature
X_i	Real values
$X_{i,c,p}$	Real values at the center point
Z_i	Coded value of the independent variable
eff	Effective
0	Initial

6- References

[1] Wu, L., Ma, T., Zang, C., Xu, Z., Sun, W., Luo, H., ... & Yao, H. (2024). Glycyrrhiza, a commonly used medicinal herb: Review of species classification, pharmacology, active ingredient biosynthesis, and synthetic biology. Journal of Advanced Research.

[2] Kaur, R., Kaur, H., & Dhindsa, A. S. (2013). Glycyrrhiza glabra: a phytopharmacological review. International journal of pharmaceutical Sciences and Research, 4(7), 2470.

[3] Rafi, M. M., Vastano, B. C., Zhu, N., Ho, C. T., Ghai, G., Rosen, R. T., ... & DiPaola, R. S. (2002). Novel polyphenol molecule isolated from licorice root (Glycrrhiza glabra) induces apoptosis, G2/M cell cycle arrest, and Bcl-2 phosphorylation in tumor cell lines. Journal of agricultural and food chemistry, 50(4), 677-684.

[4] Chin, Y. W., Jung, H. A., Liu, Y., Su, B. N., Castoro, J. A., Keller, W. J., ... & Kinghorn, A. D. (2007). Anti-oxidant constituents of the roots and stolons of licorice (Glycyrrhiza glabra). Journal of agricultural and food chemistry, 55(12), 4691-4697.

[6] Račková, L., Jančinová, V., Petríková, M., Drábiková, K., Nosáľ, R., Štefek, M., ... & Kováčová, M. (2007). Mechanism of anti-inflammatory action of liquorice extract and glycyrrhizin. Natural product research, 21(14), 1234-1241.

[7] Nakagawa, K., Kishida, H., Arai, N., Nishiyama, T., & Mae, T. (2004). Licorice flavonoids suppress abdominal fat accumulation and increase in blood glucose level in obese diabetic KK-Ay mice. Biological and Pharmaceutical Bulletin, 27(11), 1775-1778.

[8] Yin, G., Cao, L., Xu, P., Jeney, G., Nakao, M., & Lu, C. (2011). Hepatoprotective and antioxidant effects of Glycyrrhiza glabra extract against carbon tetrachloride (CCl_4)-induced hepatocyte damage in common carp (Cyprinus carpio).
[9] Mukhopadhyay, M., & Panja, P. (2008). A novel process for extraction of natural sweetener from licorice (Glycyrrhiza glabra) roots. Separation and Purification Technology, 63(3), 539-545.
[10] Simmler, C., Pauli, G. F., & Chen, S. N. (2013). Phytochemistry and biological properties of glabridin. Fitoterapia, 90, 160-184.
[11] Carmeli, E., & Fogelman, Y. (2009). Antioxidant effect of polyphenolic glabridin on LDL oxidation. Toxicology and Industrial Health, 25(4-5), 321-324.
[12] Hsieh, M. J., Chen, M. K., Chen, C. J., Hsieh, M. C., Lo, Y. S., Chuang, Y. C., ... & Yang, S. F. (2016). Glabridin induces apoptosis and autophagy through JNK1/2 pathway in human hepatoma cells. Phytomedicine, 23(4), 359-366.
[13] Fu, Y., Chen, J., Li, Y. J., Zheng, Y. F., & Li, P. (2013). Antioxidant and anti-inflammatory activities of six flavonoids separated from licorice. Food chemistry, 141(2), 1063-1071.
[14] Li, W., Asada, Y., & Yoshikawa, T. (1998). Antimicrobial flavonoids from Glycyrrhiza glabra hairy root cultures. Planta medica, 64(08), 746-747.
[15] Yu, X. Q., Xue, C. C., Zhou, Z. W., Li, C. G., Du, Y. M., Liang, J., & Zhou, S. F. (2008). In vitro and in vivo neuroprotective effect and mechanisms of glabridin, a major active isoflavan from Glycyrrhiza glabra (licorice). Life sciences, 82(1-2), 68-78.
[16] Jirawattanapong, W., Saifah, E., & Patarapanich, C. (2009). Synthesis of glabridin derivatives as tyrosinase inhibitors. Archives of pharmacal research, 32(5), 647-654.
[17] Tamir, S., Eizenberg, M., Somjen, D., Stern, N., Shelach, R., Kaye, A., & Vaya, J. (2000). Estrogenic and antiproliferative properties of glabridin from licorice in human breast cancer cells. Cancer research, 60(20), 5704-5709.
[18] Tian, M., Yan, H., & Row, K. H. (2008). Simultaneous extraction and separation of liquiritin, glycyrrhizic acid, and glabridin from licorice root with analytical and preparative chromatography. Biotechnology and bioprocess engineering, 13(6), 671-676.

[19] Tian, M., Yan, H., & Row, K. H. (2008). Extraction of glycyrrhizic acid and glabridin from licorice. International journal of molecular sciences, 9(4), 571-577.
[20] Xu, Y., Yuan, Q., Hou, X., & Lin, Y. (2009). Preparative separation of glabridin from Glycyrrhiza glabra L. extracts with macroporous resins. Separation Science and Technology, 44(15), 3717-3734.
[21] Li, X., Guo, R., Zhang, X., & Li, X. (2012). Extraction of glabridin using imidazolium-based ionic liquids. Separation and purification technology, 88, 146-150.
[22] Deyab, M. A. (2015). Egyptian licorice extract as a green corrosion inhibitor for copper in hydrochloric acid solution. Journal of Industrial and Engineering Chemistry, 22, 384-389.
[23] Xing, C., Cui, W. Q., Zhang, Y., Zou, X. S., Hao, J. Y., Zheng, S. D., ... & Li, Y. H. (2022). Ultrasound-assisted deep eutectic solvents extraction of glabridin and isoliquiritigenin from Glycyrrhiza glabra: Optimization, extraction mechanism and in vitro bioactivities. Ultrasonics Sonochemistry, 83, 105946.
[24] Qu, Q., Zhu, Z., Zhao, M., Wang, H., Cui, W., Huang, X., ... & Li, Y. (2025). Optimization ultrasonic-assisted aqueous two-phase extraction of glabridin from licorice root and its activity against the foodborne pathogen MRSA. Food Chemistry: X, 26, 102338.

[25] Hedayati, A., & Ghoreishi, S. M. (2015). Supercritical carbon dioxide extraction of glycyrrhizic acid from licorice plant root using binary entrainer: experimental optimization via response surface methodology. The Journal of Supercritical Fluids, 100, 209-217.
[26] Ghoreishi, S. M., Hedayati, A., & Mohammadi, S. (2016). Optimization of periodic static-dynamic supercritical CO2 extraction of taxifolin from pinus nigra bark with ethanol as entrainer. The Journal of Supercritical Fluids, 113, 53-60.
[27] Ahn, J., Lee, H., Jang, J., Kim, S., & Ha, T. (2013). Anti-obesity effects of glabridin-rich supercritical carbon dioxide extract of licorice in high-fat-fed obese mice. Food and chemical toxicology, 51, 439-445.
[28] Sohail, M., Rakha, A., Butt, M. S., & Asghar, M. (2018). Investigating the antioxidant potential of licorice extracts obtained through different extraction modes. Journal of Food Biochemistry, 42(2), e12466.
[29] Hong, J. H., Jung, I. I., Cho, Y. K., Haam, S., Lee, S. Y., Lim, G., & Ryu, J. H. (2019). Preparation of high-quality glabridin extract from glycyrrhiza glabra. Biotechnology and Bioprocess Engineering, 24(4), 666-674.
[30] Banafi, A., Wee, S. K., Tiong, A. N. T., Kong, Z. Y., Saptoro, A., & Sunarso, J. (2023). Modeling of supercritical fluid extraction bed: A critical review. Chemical Engineering Research and Design, 193, 685-712.
[31] Oliveira, E. L., Silvestre, A. J., & Silva, C. M. (2011). Review of kinetic models for supercritical fluid extraction. Chemical Engineering Research and Design, 89(7), 1104-1117.
[32] Ghoreishi, S. M., & Heidari, E. (2012). Extraction of epigallocatechin gallate from green tea via modified supercritical CO2: Experimental, modeling and optimization. The Journal of supercritical fluids, 72, 36-45.
[33] Ghoreishi, S. M., Hedayati, A., & Mousavi, S. O. (2016). Quercetin extraction from Rosa damascena Mill via supercritical CO2: Neural network and adaptive neuro fuzzy interface system modeling and response surface optimization. The Journal of Supercritical Fluids, 112, 57-66.
[34] Daraee, A., Ghoreishi, S. M., & Hedayati, A. (2019). Supercritical CO2 extraction of chlorogenic acid from sunflower (Helianthus annuus) seed kernels: modeling and optimization by response surface methodology. The Journal of Supercritical Fluids, 144, 19-27.
[35] Czitrom, V. (1999). One-factor-at-a-time versus designed experiments. The American Statistician, 53(2), 126-131.
[36] Khuri, A. I., & Mukhopadhyay, S. (2010). Response surface methodology. Wiley interdisciplinary reviews: Computational statistics, 2(2), 128-149.
[37] Song, Q., Zhu, J., Wan, J., & Cao, X. (2010). Measurement and modeling of epigallocatechin gallate solubility in supercritical carbon dioxide fluid with ethanol cosolvent. Journal of Chemical & Engineering Data, 55(9), 3946-3951.
[38] Peng, D. Y., & Robinson, D. B. (1976). A new two-constant equation of state. Industrial & Engineering Chemistry Fundamentals, 15(1), 59-64.
[39] E. Bruce, J.M. Prausnitz, P.O. John, Properties of Gases and Liquids, 5th ed.,McGraw-Hill, New York, 2001, pp. 467–564, 635–691.
[40] Abaroudi, K., Trabelsi, F., Calloud-Gabriel, B., & Recasens, F. (1999). Mass transport enhancement in modified supercritical fluid. Industrial & engineering chemistry research, 38(9), 3505-3518.
[41] Ghoreishi, S. M., & Akgerman, A. (2004). Dispersion coefficients of supercritical fluid in fixed beds. Separation and Purification Technology, 39(1-2), 39-50.

[42] Tan, C. S., Liang, S. K., & Liou, D. C. (1988). Fluid—solid mass transfer in a supercritical fluid extractor. The Chemical Engineering Journal, 38(1), 17-22.
[43] Wakao, N., & Smith, J. M. (1962). Diffusion in catalyst pellets. Chemical Engineering Science, 17(11), 825-834.
[44] Mehl, A., Nascimento, F. P., Falcao, P. W., Pessoa, F. L., & Cardozo-Filho, L. (2011). Vapor-Liquid Equilibrium of Carbon Dioxide+ Ethanol: Experimental Measurements with Acoustic Method and Thermodynamic Modeling. Journal of Thermodynamics, 2011(1), 251075.

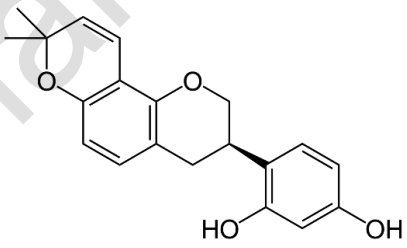

Fig. 1

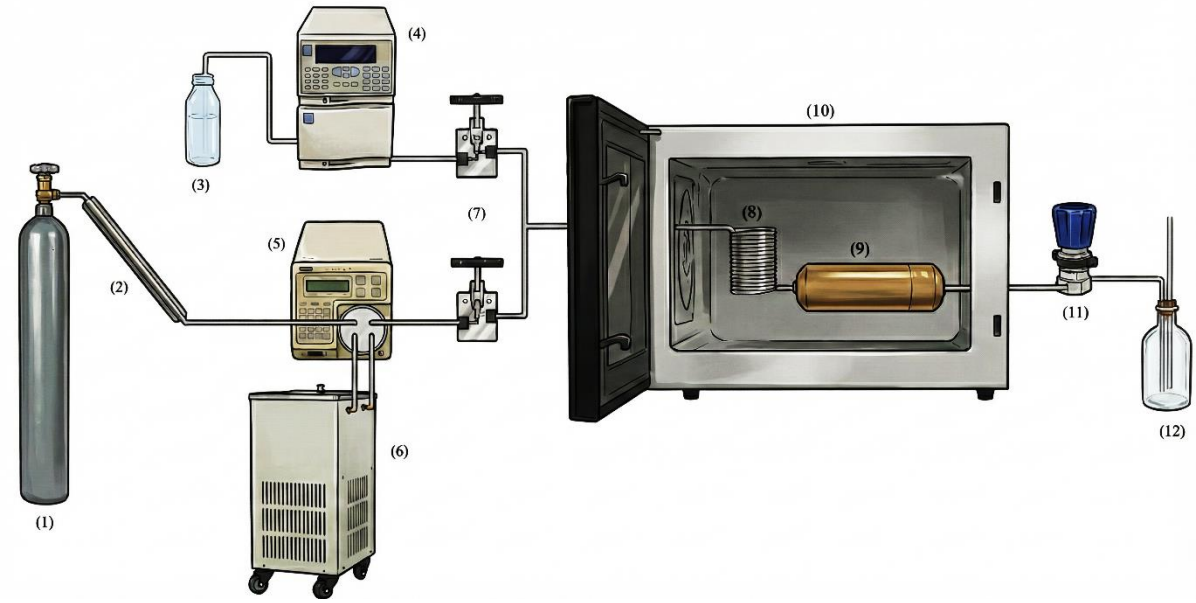

Fig. 2

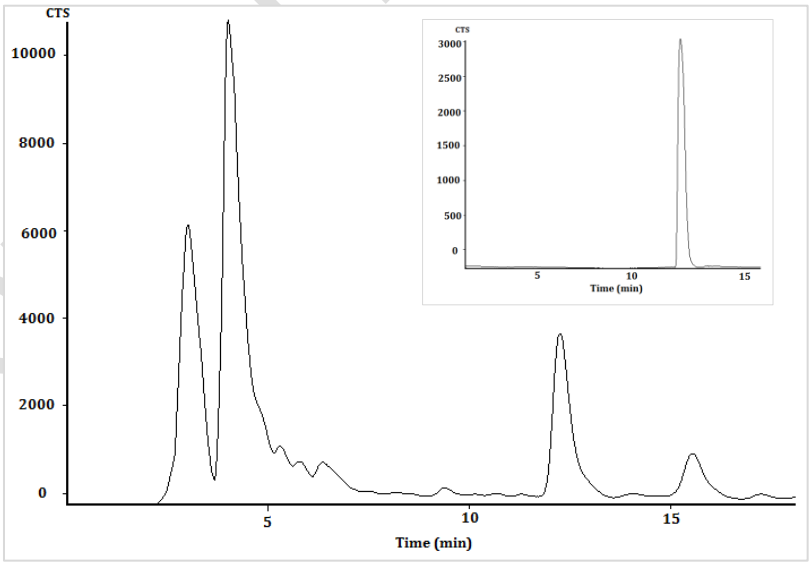

Fig. 3

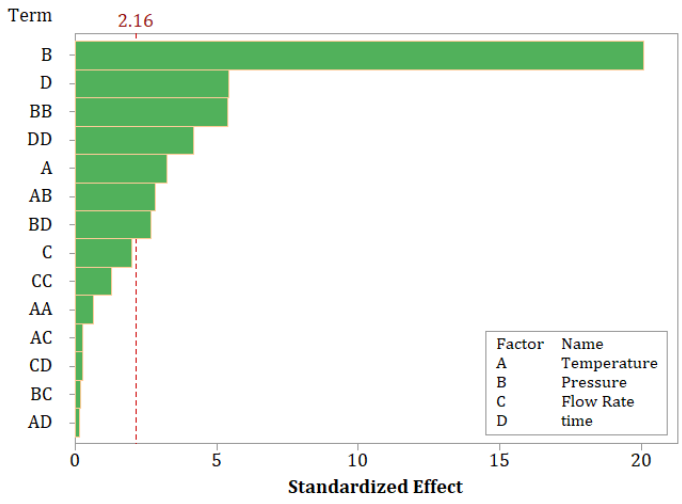

Fig. 4

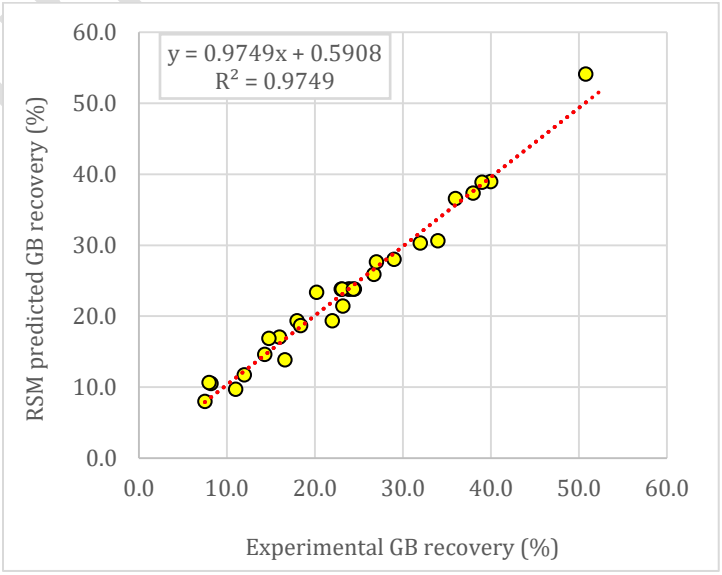

Fig. 5

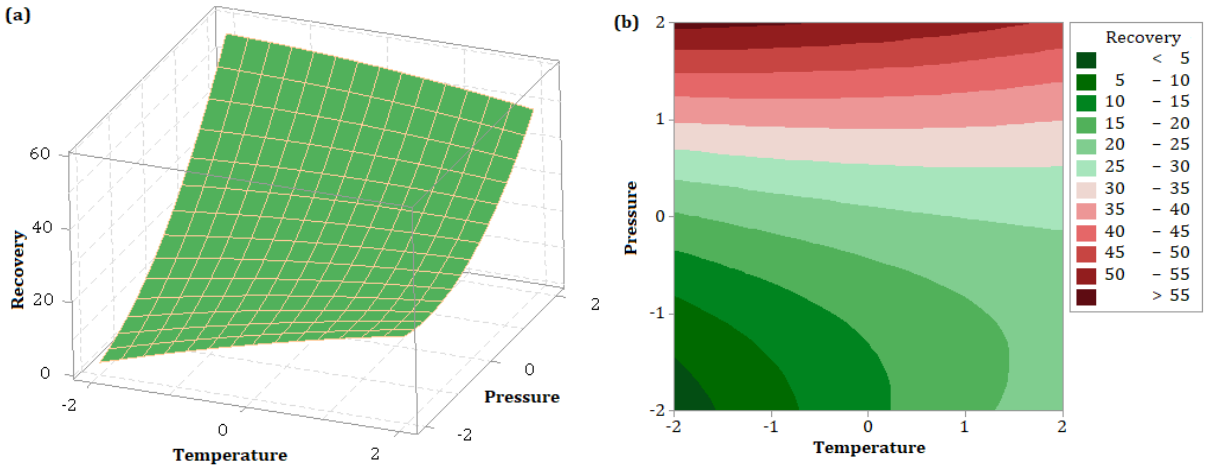

Fig. 6

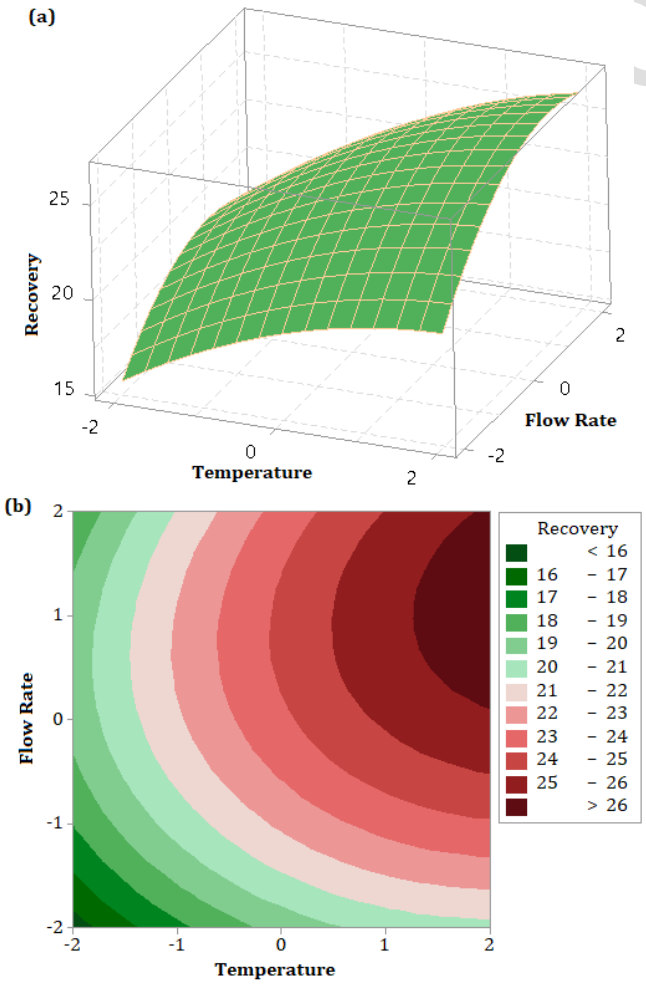
(a)
Recovery
25
20
15
-2
0
2
Temperature
Flow Rate
(b)
Flow Rate
Temperature
Recovery
< 16
16 – 17
17 – 18
18 – 19
19 – 20
20 – 21
21 – 22
22 – 23
23 – 24
24 – 25
25 – 26
> 26

Fig. 7

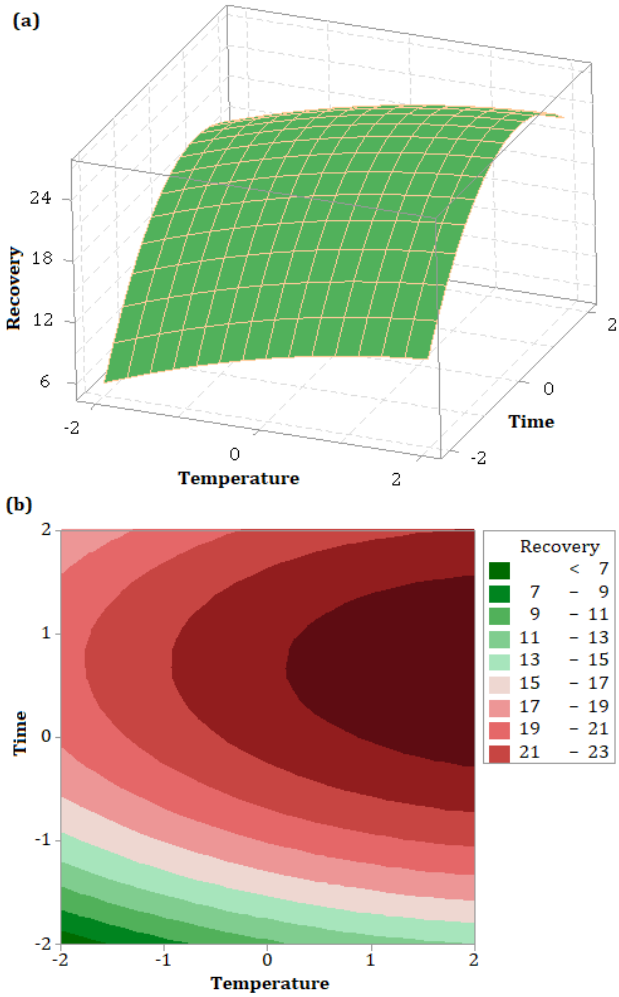

Fig. 8

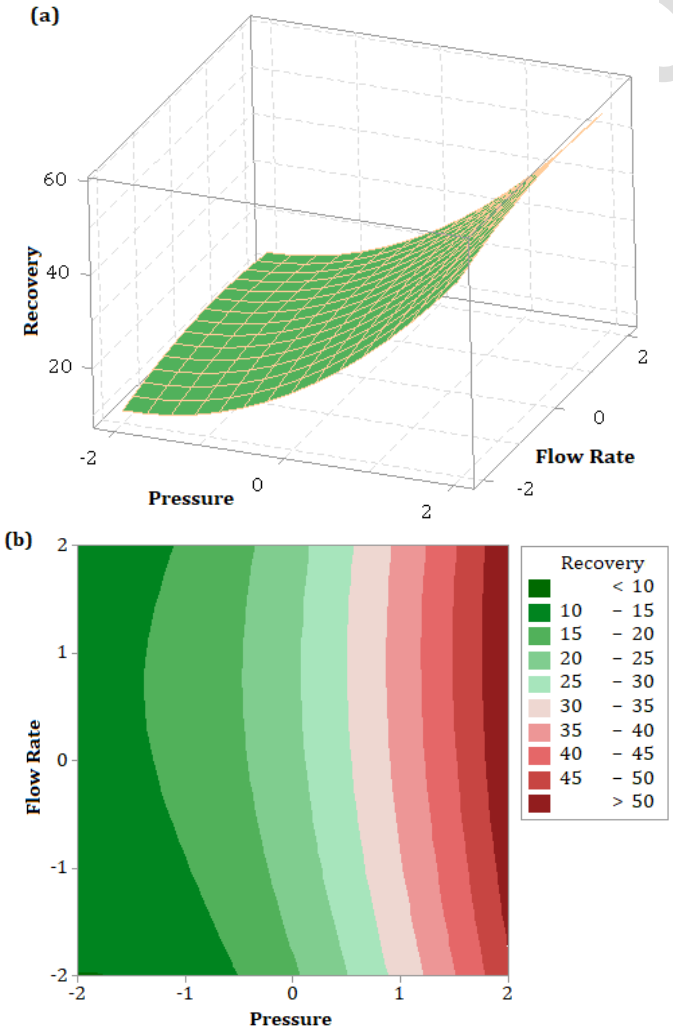

Fig. 9

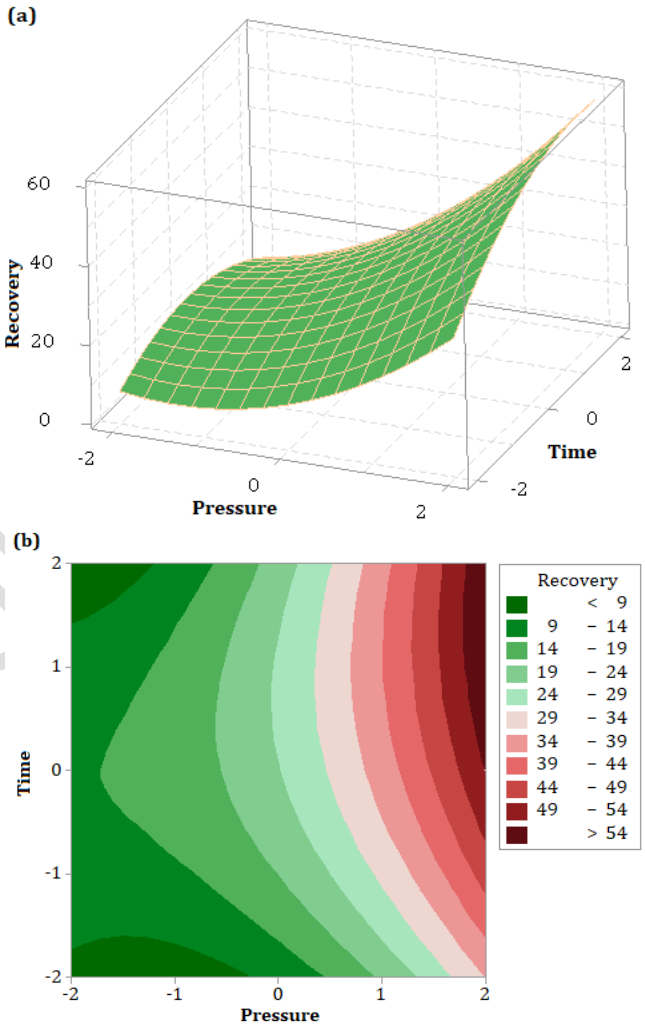
(a)
Recovery
60
40
20
0
-2
0
2
Pressure
-2
0
2
Time
(b)
Time
2
1
0
-1
-2
-2
-1
0
1
2
Pressure
Recovery
< 9
9 – 14
14 – 19
19 – 24
24 – 29
29 – 34
34 – 39
39 – 44
44 – 49
49 – 54
> 54

Fig. 10

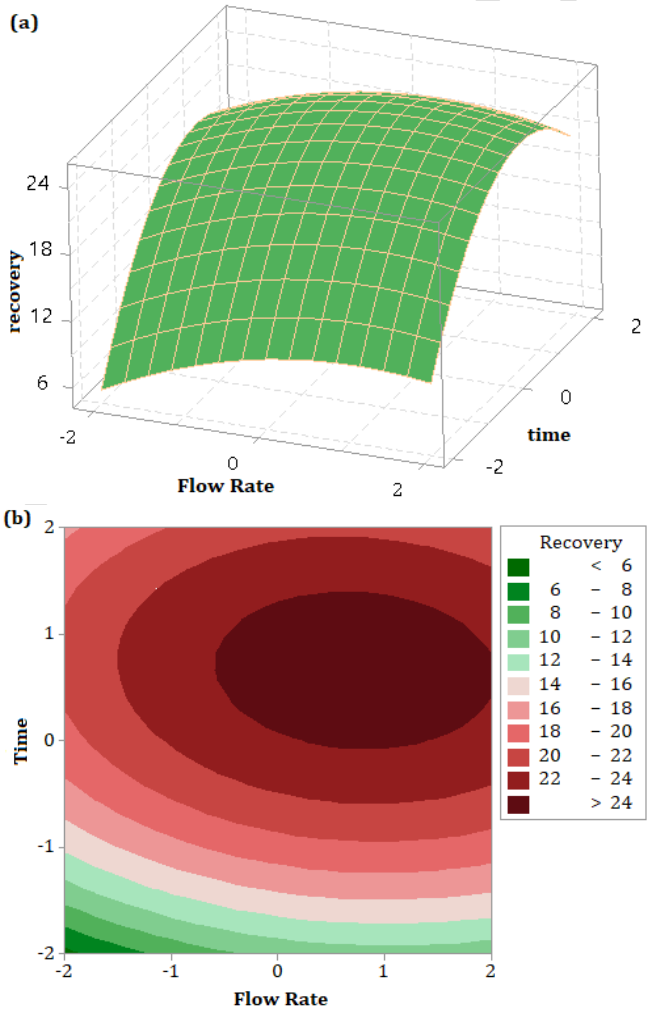
(a)
recovery
24
18
12
6
-2
0
2
Flow Rate
-2
0
2
time
(b)
Time
2
1
0
-1
-2
-2
-1
0
1
2
Flow Rate
Recovery
< 6
6 – 8
8 – 10
10 – 12
12 – 14
14 – 16
16 – 18
18 – 20
20 – 22
22 – 24
> 24

Fig. 11

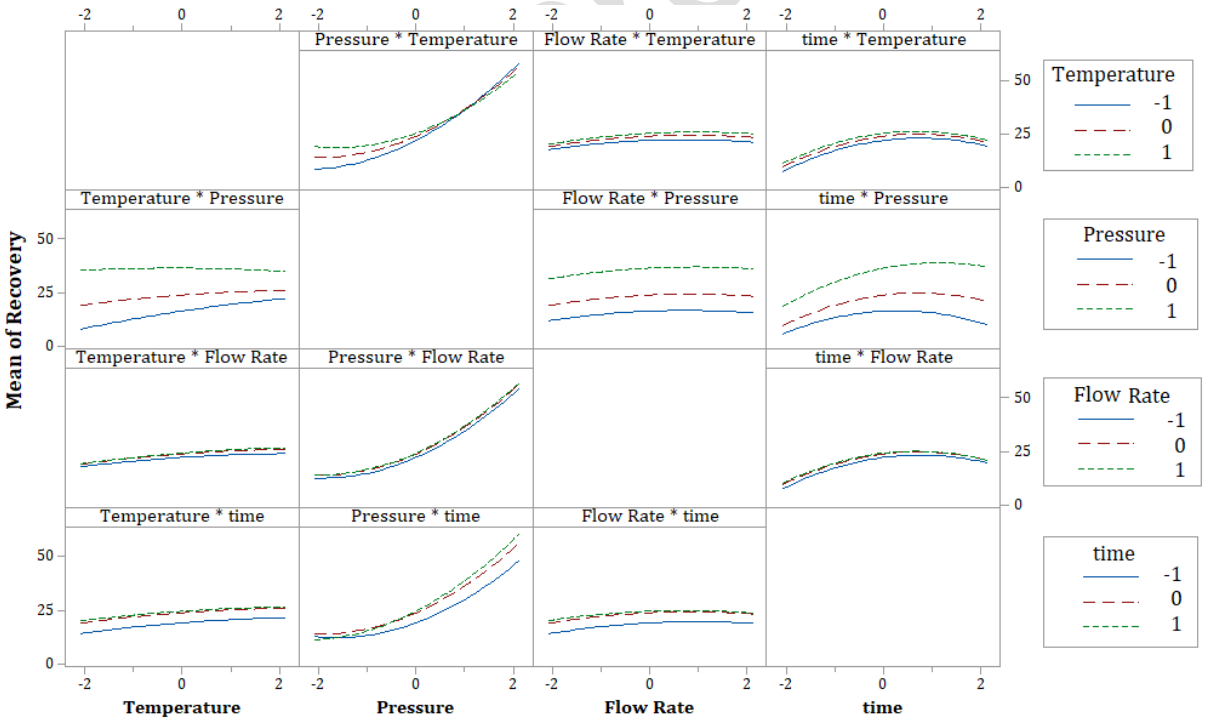

Fig. 12

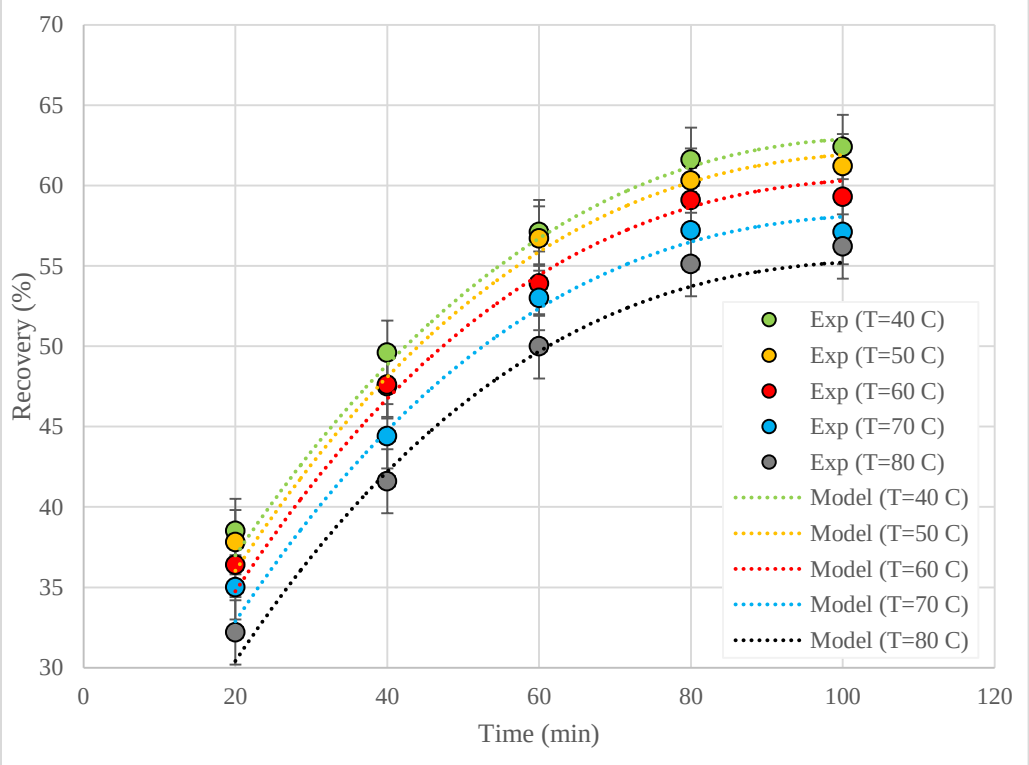

Fig. 13

Table 1: Independent variables in RSM based on coded and uncoded levels.

Coded variables	Temperature [ºC]	Pressure [MPa]	Dynamic extraction time [min]	CO_2 flow rate [ml/min]
-2	40	8	20	0.5
-1	50	12	40	1
0	60	16	60	1.5
+1	70	20	80	2
+2	80	24	100	2.5

Table 2: RSM designed experiments for GB extraction from licorice plant root and observed experimental and modeling results.

Number of experiments	Temperature (*T*)	Pressure (*P*)	Flow Rate (*Q*)	Time (*t*)	*R* (Experiment)	*R* (RSM model)
1	-2	0	0	0	18.0	19.3
2	0	-2	0	0	16.6	13.8
3	0	0	0	0	23.8	23.8
4	2	0	0	0	26.7	25.9
5	0	0	2	0	20.2	23.4
6	0	0	0	0	23.0	23.8
7	0	0	0	2	23.2	21.4
8	0	2	0	0	50.8	54.1
9	0	0	0	-2	8.2	10.5
10	0	0	-2	0	22.0	19.3
11	1	-1	-1	-1	14.3	14.6
12	0	0	0	0	24.0	23.8
13	-1	-1	1	-1	11.0	9.7
14	-1	-1	-1	1	8.0	10.6
15	-1	1	-1	-1	29.0	28.0
16	1	1	-1	1	36.0	36.5
17	1	-1	1	1	18.4	18.6
18	1	1	1	-1	34.0	30.6
19	-1	1	1	1	40.0	38.9
20	0	0	0	0	24.5	23.8
21	0	0	0	0	23.1	23.8

22	1	-1	1	-1	16.0	17.0
23	1	-1	-1	1	14.8	16.9
24	-1	-1	1	1	12.0	11.7
25	1	1	-1	-1	27.0	27.6
26	-1	-1	-1	-1	7.5	8.0
27	1	1	1	1	39.0	38.8
28	-1	1	-1	1	38.0	37.3
29	-1	1	1	-1	32.0	30.3
30	0	0	0	0	24.4	23.8

Table 3: Regression coefficients and ANOVA of the second-order polynomial model for glabridin extraction recovery.

Source	DF[1]	Coef[2]	SE Coef[3]	Adj SS[4]	Adj MS[5]	T-value	F-Value	P-Value
Model	16			3136.37	196.02		32.57	0.000
Constant		23.80	1.00			23.76		0.000
Blocks	2			2.52	1.26		0.21	0.813
1		0.403	0.633			0.64		0.535
2		-0.137	0.633			-0.22		0.833
Linear	4			2695.38	673.85		111.97	0.000
T	1	1.642	0.501	64.68	64.68	3.28	10.75	0.006
P	1	10.058	0.501	2428.08	2428.08	20.09	403.47	0.000
Q	1	1.008	0.501	24.40	24.40	2.01	4.05	0.065
t	1	2.725	0.501	178.22	178.22	5.44	29.61	0.000
Square	4			343.87	85.97		14.28	0.000
T^2	1	-0.304	0.468	2.54	2.54	-0.65	0.42	0.527
P^2	1	2.533	0.468	176.03	176.03	5.41	29.25	0.000
Q^2	1	-0.617	0.468	10.43	10.43	-1.32	1.73	0.211
t^2	1	-1.967	0.468	106.09	106.09	-4.20	17.63	0.001
2-Way Interaction	6			94.60	15.77		2.62	0.069
T×*P*	1	-1.750	0.613	49.00	49.00	-2.85	8.14	0.014
T×*Q*	1	0.175	0.613	0.49	0.49	0.29	0.08	0.780
T×*t*	1	-0.100	0.613	0.16	0.16	-0.16	0.03	0.873
P×*Q*	1	0.137	0.613	0.30	0.30	0.22	0.05	0.826
P×*t*	1	1.662	0.613	44.22	44.22	2.71	7.35	0.018
Q×*t*	1	-0.163	0.613	0.42	0.42	-0.26	0.07	0.795
Error	13			78.23	6.02			

Lack-of-Fit	10			76.94	7.69		17.89	0.18
Pure Error	3			1.29	0.43			
Total	29			3214.60				

[1]degrees of freedom; [2]regression coefficient; [3]The standard error of the coefficient; [4]Adjusted sums of squares; [5]Adjusted mean squares